Molecular Biology of the Cell
Vol. 11, 1815–1827, May 2000

Intercellular Calcium Waves in HeLa Cells Expressing GFP-labeled Connexin 43, 32, or 26

Koen Paemeleire,* Patricia E. M. Martin,† Sharon L. Coleman,† Kevin E. Fogarty,‡ Walter A. Carrington,‡ Luc Leybaert,* Richard A. Tuft,‡ W. Howard Evans,† and Michael J. Sanderson‡§

‡Department of Physiology, University of Massachusetts Medical School, Worcester, Massachusetts 01655; *Department of Physiology and Pathophysiology, University of Ghent, B-9000 Ghent, Belgium; and †Department of Medical Biochemistry, University of Wales College of Medicine, Cardiff CF4 4XN, Wales, United Kingdom

Submitted August 27, 1999; Revised January 10, 2000; Accepted January 28, 2000
Monitoring Editor: Paul T. Matsudaira

This study was undertaken to obtain direct evidence for the involvement of gap junctions in the propagation of intercellular Ca^{2+} waves. Gap junction-deficient HeLa cells were transfected with plasmids encoding for green fluorescent protein (GFP) fused to the cytoplasmic carboxyl termini of connexin 43 (Cx43), 32 (Cx32), or 26 (Cx26). The subsequently expressed GFP-labeled gap junctions rendered the cells dye- and electrically coupled and were detected at the plasma membranes at points of contact between adjacent cells. To correlate the distribution of gap junctions with the changes in $[Ca^{2+}]_i$ associated with Ca^{2+} waves and the distribution of the endoplasmic reticulum (ER), cells were loaded with fluorescent Ca^{2+}-sensitive (fluo-3 and fura-2) and ER membrane (ER-Tracker) dyes. Digital high-speed microscopy was used to collect a series of image slices from which the three-dimensional distribution of the gap junctions and ER were reconstructed. Subsequently, intercellular Ca^{2+} waves were induced in these cells by mechanical stimulation with or without extracellular apyrase, an ATP-degrading enzyme. In untransfected HeLa cells and in the absence of apyrase, cell-to-cell propagating $[Ca^{2+}]_i$ changes were characterized by initiating Ca^{2+} puffs associated with the perinuclear ER. By contrast, in Cx–GFP-transfected cells and in the presence of apyrase, $[Ca^{2+}]_i$ changes were propagated without initiating perinuclear Ca^{2+} puffs and were communicated between cells at the sites of the Cx–GFP gap junctions. The efficiency of Cx expression determined the extent of Ca^{2+} wave propagation. These results demonstrate that intercellular Ca^{2+} waves may be propagated simultaneously via an extracellular pathway and an intracellular pathway through gap junctions and that one form of communication may mask the other.

INTRODUCTION

Intercellular Ca^{2+} waves have been found to occur in a wide variety of cell types (Cornell-Bell and Finkbeiner, 1991; Sanderson *et al.*, 1994; Kasai, 1995; Robb-Gaspers and Thomas, 1995; Charles, 1998). Intercellular Ca^{2+} waves can be induced by electrical, chemical, and mechanical stimuli and consist of an increase in the intracellular free Ca^{2+} concentration ($[Ca^{2+}]_i$) in the stimulated cell that is communicated through consecutive rows of neighboring cells (Sanderson *et al.*, 1990; Charles *et al.*, 1991; Hassinger *et al.*, 1996). Studies aimed at elucidating the mechanisms underlying the propagation of waves have led to the hypothesis that IP_3 acts as a Ca^{2+}-mobilizing messenger and diffuses through gap junctions between neighboring cells (Sanderson, 1995; Leybaert *et al.*, 1998a). Alternatively, Ca^{2+} itself may diffuse through gap junctions and trigger the release of Ca^{2+} from IP_3-sensitized IP_3 receptors (Robb-Gaspers and Thomas, 1995; Zimmermann and Walz, 1999). Either scenario requires the presence of gap junctions.

Gap junction channels are formed from two hexameric hemichannels, called connexons, that are embedded in opposing plasma membranes and assembled from six protein monomers or connexins (Cxs) arranged around a central pore. Connexins are a family of 15 proteins (in rodents) that are classified on the basis of their molecular weight and structure (Kumar and Gilula, 1992; Yeager *et al.*, 1998). Perhaps the most commonly studied gap junctional proteins are Cx26, Cx32, and Cx43 (Simon and Goodenough, 1998; Si-

§ Corresponding author. E-mail address: michael.sanderson@umassmed.edu.

mon, 1999). The relationship between gap junctions and Ca^{2+} waves has been examined previously, and it was found that C6 glioma cells, which have nonfunctional gap junctions, transmitted Ca^{2+} waves only after transfection with Cx43 (Charles *et al*., 1992). Similarly, Toyofuku *et al*. (1998) have shown that expression of Cx43 in the human embryonic kidney cell line, HEK293, is required to propagate intercellular Ca^{2+} waves. In addition, blockers of gap junctional communication, such as halothane, octanol, α-glycyrrhetinic acid, and antibodies, significantly reduce the propagation distance of intercellular Ca^{2+} waves (Sanderson *et al*., 1990; Finkbeiner, 1992; Venance *et al*., 1997; Boitano *et al*., 1998), whereas fast superfusion did not bias the propagation of calcium waves in the direction of the flow (Hansen *et al*., 1993; Churchill *et al*., 1996).

Although a role for gap junctions in the propagation of Ca^{2+} waves is well supported, Ca^{2+} waves may also be propagated by the release of an extracellular messenger such as ATP. These waves are able to cross discontinuities in the cell culture, are biased by extracellular fluid flows, and are inhibited by the ATP-degrading enzyme apyrase (Osipchuk and Cahalan, 1992; Furuya *et al*., 1993; Hassinger *et al*., 1996; Guthrie *et al*., 1999). This ability to release and respond to ATP also appears to be linked to the expression of gap junctions, because forced overexpression of gap junctions was suggested to increase the amount of ATP released by HeLa and C6 glioma cells transfected with Cx43 (Cotrina *et al*., 1998). As a result, the mechanism of Ca^{2+} wave propagation in transfected cells is more complicated and may occur via both ATP and gap junctions.

Because the subcellular characteristics should indicate the mechanism of the propagating Ca^{2+} waves, i.e., whether they move intracellularly or extracellularly, we directly studied the involvement of gap junctions in intercellular Ca^{2+} wave propagation by using green fluorescent protein (GFP) to visualize the location of specific gap junctions in live HeLa cells. Cells were transfected with plasmids that resulted in the expression of GFP-labeled connexin 43 (Cx43), connexin 32 (Cx32), or connexin 26 (Cx26), and the intercellular Ca^{2+} waves in these cells were analyzed with digital microscopy. Although there are numerous types of connexins that exist in various tissues, we limited this study to connexins 43, 32, and 26 because these connexins are the predominate forms in the epithelial and glial cells in which intercellular Ca^{2+} waves have been extensively observed. In addition, we correlated the distribution of the endoplasmic reticulum with elemental and global intracellular Ca^{2+} events that were observed during wave propagation. Using these techniques, we demonstrate that both modes of Ca^{2+} wave propagation, that is, intercellular propagation through gap junctions and extracellular propagation by ATP diffusion, can occur simultaneously in GFP–connexin-transfected HeLa cells.

MATERIALS AND METHODS

Materials

Cell culture reagents and plasticware were obtained from Life Technologies (Grand Island, NY), molecular biology reagents were obtained from Promega (Madison, WI) and other reagents were obtained from Sigma (St. Louis, MO) unless stated otherwise.

Construction of Chimeric Connexin–GFP cDNA

Cx26, Cx32, and Cx43 cDNA were fused inframe to the amino terminus of enhanced GFP (EGFP) in the vector pEGFP-N1 as follows. The ORF of Cx26, Cx32, and Cx43 was initially amplified by PCR from plasmids containing the relevant full-length cDNA using the appropriate oligonucleotide primers that introduced *Bgl*II (for Cx43 and Cx26 constructs) and *Hin*dIII restriction enzyme sites (for Cx32 constructs) at the 5′ and 3′ end of the cDNA. The primers used were as follows (restriction enzyme sites are underlined; Cx sequences are in bold): Cx43 forward primer Cx43GF: 5′ CTA CCG GAC TCA GAT CTC **ATG GGT GAC TGG AGT;** Cx43 reverse primer Cx43GR: 5′ CTT GAG CTC GAG ATC TGA **AAT CTC CAG GTC ATC;** Cx32 forward primer Cx32GF: 5′ CTC GAG CTC AAG CTT **ATG AAC TGG ACA GGT;** Cx32 reverse primer Cx32GR: 5′ CAG AAT TCG AAG CTT **GCA GGC TGA GCA TCG;** Cx26 forward primer Cx26GF: 5′ CTA CCG GAC TCA GAT CTC **ATG GAT TGG GGC ACC;** Cx26 reverse primer Cx26GR: 5′ CTT GAG CTC GAG ATC TGA **GAC TGG TCT TTT GGA.**

To generate the Cx–GFP chimeric constructs, the resulting PCR products were digested with *Bgl*II or *Hin*dIII and ligated into the *Bgl*II or *Hin*dIII site of pEGFP-N1 (Clontech, Basingstoke, Hampshire, United Kingdom) (Sambrook *et al*., 1989) followed by transformation into *Escherichia coli* (DH5α). Identification of positive clones was achieved by miniplasmid preparation and restriction enzyme analysis. Selected constructs were sequenced using the PRISM Dye Termination Cycle Sequencing kit (Perkin Elmer-Cetus, Beaconsfield, Buckinghamshire, United Kingdom).

Establishment of Stable HeLa Cell Populations Expressing Cx–GFP Proteins

HeLa Ohio cells (ECACC, Salisbury, Wiltshire, United Kingdom) were cultured in DMEM supplemented with 10% fetal calf serum, penicillin/streptomycin (100 μg/ml), amphotericin (100 μg/ml), and L-glutamine (2 mM). Subconfluent monolayers (4×10^6 cells in 100-mm dishes) were transfected with 10 μg of the relevant Cx–GFP cDNA by calcium phosphate (Martin *et al*., 1998). Forty-eight hours after transfection, cells were transferred to medium supplemented with 4 mg/ml Geneticin (antibiotic G418-sulfate) and cultured for ~3 wk. After significant cell death had occurred and the surviving cells were growing well in Geneticin, cells positive for GFP fluorescence were separated and collected with a fluorescence-activated cell sorter (Becton Dickinson, San Jose, CA). The GFP-positive cell populations were maintained in complete DMEM supplemented with 4 mg/ml Geneticin. Separate media were prepared for nontransfected HeLa (further called HeLa control cells), HeLa Cx26, HeLa Cx32, and HeLa Cx43 cells, respectively, to avoid contamination of different strains of cells. Stocks of cells were split at a ratio of 1:10 once a week and used for up to seven passages. For Ca^{2+} imaging experiments, cells were grown on glass-bottom Petri dishes (Mattek, Ashland, MA). Eighteen hours before experiments, Cx–GFP expression was enhanced by addition of 5 mM sodium butyrate to the medium (Wilkinson and Akrigg, 1992; George *et al*., 1998b).

Western Blot Analysis

HeLa cells (ECACC) were transfected with cDNA encoding for Cx43–GFP chimerae and harvested for Western blot analysis as described by Martin *et al*., (1998). Proteins were detected with either a primary rabbit antibody generated against amino acid sequences in the carboxyl tail of the Cx43 (Gap33, amino acids 314–325) or a polyclonal antibody against GFP (Clontech) and a secondary goat anti-rabbit antibody conjugated to horseradish peroxidase (Bio-Rad, Hemel Hempstead, Hertfordshire, United Kingdom). Blots were developed using the enhanced chemiluminescence system (Pierce, Chester, Cheshire, United Kingdom).

Immunolocalization of Connexin–GFP Proteins

Cells (1×10^5) were seeded on 16-mm^2 coverslips overnight and fixed the next day in 4% formaldehyde and processed for immunocytochemical analysis as described (Martin *et al.*, 1998). Colocalization of Cx and GFP fluorescence was confirmed by staining the cells with the relevant primary antibodies. For Cx26 and Cx32, commercially available monoclonal antibodies (Chemicon, Harrow, United Kingdom) against the intracellular loop were used; for Cx 43, a polyclonal antibody, raised in rabbits, against the carboxyl tail was used (Gap 33; Diez *et al.*, [1999]). The secondary antibody was either goat anti-rabbit or goat anti-mouse IgG conjugated to Cy3. Cells were mounted in Fluorsave (Calbiochem, Beeston, Nottingham, United Kingdom) to preserve fluorescence and viewed on a Leitz DMBRE confocal microscope.

Assessment of Efficiency of Expression

The expression of Cx43–GFP, Cx32–GFP and Cx26–GFP was quantified by averaging imaging data from 15 different areas (320×240 μm) obtained from the respective confluent monolayers of passage 4 HeLa cells. To obtain the area of Cxs, images were recorded and thresholded to separate the GFP fluorescence from background, and all pixels with values above the threshold were counted. This number was divided by the total number of pixels in the field of view and expressed as a percentage.

Assessment of Dye and Electrical Coupling

Confluent monolayers of HeLa cells expressing the chimeric Cx–GFP constructs were microinjected with Lucifer yellow (5% wt/vol in 0.3 M LiCl). Fifteen minutes after injection, cells were fixed in 4% formaldehyde and viewed on a Zeiss Axiostat microscope. The dye-coupling efficiency was calculated as the percentage of cells, injected with Lucifer yellow, that transferred dye to five or more neighboring cells. Electrical coupling was measured in isolated cell pairs with two microelectrodes pulled from glass capillaries (1.2-mm outer diameter; A-M Systems, Carlsbourg, WA), with resistances ~50–100 MΩ. Electrodes were connected to a balanced bridge circuit (Cyto 721, World Precision Instruments, Sarasota, FL) and served to inject current and measure potential. Current was injected as 1-nA square pulses of 200 ms duration at a frequency of 2 Hz (I_1). The resulting changes in membrane potential in the injected cell (V_1) and the adjacent cell (V_2) were measured, and the electrical coupling ratio (V_2/V_1) was calculated.

Experimental Solutions

Experiments were performed in HBSS supplemented with 25 mM HEPES and brought to pH 7.4 (HBSS–HEPES) with or without apyrase (Grade III) as required. A stock solution of apyrase was prepared in distilled H_2O at 2000 IU/ml and further diluted in HBSS–HEPES to yield a final concentration of 40 IU/ml. Whenever apyrase was used in the experiments, cultures were preincubated in apyrase solution for 30 min.

Mechanical Stimulation

A glass pipette with a tip diameter of ~1 μm was pulled from a glass capillary (1.5-mm outer diameter; A-M Systems) and mounted on a piezo-electric device that was driven by a single square pulse of 3 V and 150 ms duration. The height of the pipette tip was adjusted such that it gently touched the cell membrane of a single cell upon activation of the piezo-electric device. A stronger mechanical stimulus was applied to the cells by lowering the glass pipette ~1 μm so that it distorted the cell to a great extent.

Measurements of Intracellular Free Ca^{2+} Concentration

Initial experiments were performed with digital video microscopy and an epifluorescence microscope as described elsewhere (Lansley and Sanderson, 1999). HeLa cells were loaded with the Ca^{2+}-sensitive dye fura-2 AM (Molecular Probes, Eugene, OR) (5 μM in HBSS–HEPES for 30 min at 37°C followed by deesterification at room temperature for 30 min). The fura-2 loaded cultures were observed on an inverted microscope (Nikon Diaphot 300) with a 40× oil immersion objective. The video field of view measured 320×240 μm. Cells were excited by light emitted from a Hg arc lamp and filtered with excitation filters (center wavelengths of 340 and 380 nm). Excitation light was separated from the light emitted from the specimen using a 400-nm dichroic mirror. Emitted light was collected through an emission filter (center wavelength of 515 nm) by a silicon intensified target camera. Images were recorded at video rate (30 fps) by an optical memory disk recorder (OMDR) and analyzed using custom-written software (Leybaert *et al.*, 1998b).

Studies requiring higher temporal and spatial resolution were performed on a digital high-speed microscope (Figure 1) that is described in detail elsewhere (Rizzuto *et al.*, 1998; Kidd *et al.*, 1999; ZhuGe *et al.*, 1999). For high-resolution experiments, HeLa cells were loaded with the Ca^{2+}-sensitive fluoroprobe fluo-3 AM (Molecular Probes) (5 μM in HBSS–HEPES for 30 min at 37°C followed by deesterification at room temperature for 30 min). Fluo-3–loaded cells were viewed with a 60× NA 1.4 oil immersion lens (Nikon). The cells were excited by the 488 nm line of an Argon laser expanded to provide wide-field illumination of the specimen. Emitted fluorescence was collected using a 510-nm long-pass emission filter and a cooled CCD camera, at a maximal frequency of 100 images per second. Because of a storage limit of 200 images, the duration of recordings was 2 s at 100 images per second. Slower image collection rates were used to increase the duration of recordings. Each pixel represents an area of 333×333 nm. The dimensions of each image were 42.6×42.6 μm (128×128 pixels). An in situ calibration was investigated for fura-2–loaded cells by exposing them to known Ca^{2+} concentrations in the presence of 100 μM ionomycin and 10 μM thapsigargin. These calibrations confirmed previous observations that there is a difference in the apparent K_D of fura-2 in the nucleus and cytoplasm (Perez-Terzic *et al.*, 1997), a situation that is incompatible with the calibration formula described by Grynkiewicz *et al.* (1985). Therefore the fura-2 data were not transformed to $[Ca^{2+}]_i$ values but were represented in arbitrary Ca^{2+} units using estimated values from calibration experiments for the parameters R_{min} (0.1), R_{max} (5.0), and F_oF_s (6.0). The fluo-3 data are represented as relative changes in fluorescence ($\Delta F/F$ or $(F_t - F_0)/F_0$, where F_t is the fluorescence at time = t and F_0 is the fluorescence at time = 0). Data are represented either as two-dimensional maps with a pseudocolor scale or with respect to time from 2.3×2.3 μm analysis points (7×7 pixels).

ER-Tracker, Mito-Tracker, and Connexin–GFP Image Acquisition and Deconvolution

Cells loaded with fluo-3 were subsequently loaded with either ER-Tracker Blue-White DPX (ER-Tracker) or Mito-Tracker Red CM-H_2Ros (Mito-Tracker; both from Molecular Probes). Stock solutions of ER-Tracker and Mito-Tracker were prepared at 1 mM in DMSO. Cells were loaded for 30 min at 37°C with 100 nM of either ER-Tracker or Mito-Tracker in prewarmed culture medium. The ER-Tracker, Mito-Tracker, and Cx–GFP fluorescence were imaged on a digital high-speed microscope by exciting the specimen with 386 nm (UV laser), 514 nm, or 488 nm (tuned visible laser) light, respectively. Fluorescence images were taken for each dye at 51 sequential focal planes separated by 0.25 μm. The focus changes were achieved by moving the microscope stage with a piezo-electric translator (Figure 1). Point-spread functions were obtained from 189 nm fluorescein-coated beads. A dark-current image was obtained from a

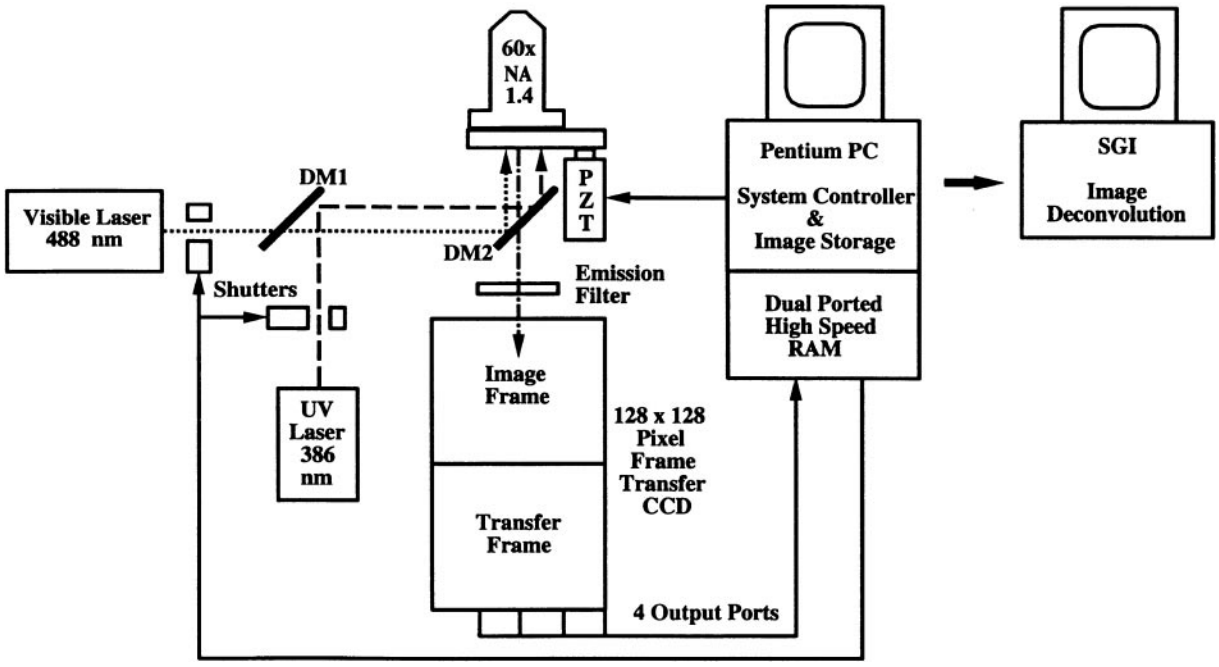

Figure 1. A schematic of the digital high-speed microscope. The specimen is either excited with 488 or 514 nm wavelength light from an argon–krypton laser (visible laser) or by 386 nm wavelength light from an argon laser (UV laser). The laser beams pass through beam expansion and collection optics to provide wide-field illumination. Shutters operated by a Pentium PC control the exposure to the lasers. The excitation beams are directed to the specimen by two dichroic mirrors (DM1 400 nm; DM2 505 nm). The specimen is viewed with a 60× NA 1.4 oil objective lens with the numerical aperture set at 1.4. The fluorescence emitted from the specimen is filtered by a 510 nm long-pass emission filter and is captured by a high-speed, 128 × 128 pixel frame transfer CCD camera. The 12-bit output is read out through four ports and stored on two high-speed data capture boards, each with 4 megabytes of dual-ported RAM. When the RAM is filled with 200 images, the data are transferred to the hard disk in a Pentium PC. This PC also controls the advancement of the piezo-electric translator (PZT) when images at multiple focal planes throughout the specimen are acquired. Images are transferred from the Pentium PC to a Silicon Graphics Imaging (SGI) facility for image deconvolution and analysis.

HBSS–HEPES-filled glass-bottom Petri dish. The images of ER-Tracker, Mito-Tracker, and Cx-GFP were digitally restored by subtracting dark currents and removing the out-of-focus light using the point spread function and a deconvolution algorithm described by Carrington *et al*. (1995).

RESULTS

Distribution and Function of Cx–GFP Gap Junctions

The cellular location of the Cx–GFP proteins was determined by the fluorescent properties of the GFP. Analysis by confocal microscopy showed that GFP chimerae of wild-type Cx26, Cx32, and Cx43 were targeted to the plasma membrane to produce a punctate staining typical for gap junctions. Cx–GFP expression varied considerably from cell to cell. For immunolocalization studies, cells expressing numerous gap junctions were analyzed; however, to simplify the correlation of Ca^{2+} waves with specific gap junctions, cells expressing only one to five Cx–GFP plaques between neighboring cells were used. Immunolocalization studies using site-specific antibodies to Cx43 demonstrated that the GFP fluorescence coincided with the Cx–antibody fluorescence, confirming that GFP identified the location of the gap junctions (Figure 2). Similar results were obtained with Cx26 and Cx32 (our unpublished data).

Western blot analysis indicated that HeLa cells transfected with Cx43–GFP expressed a chimeric protein of the predicted molecular mass (~71 kDa) when probed with either the antibody to Cx43 (Gap33) or the antibody to GFP (Figure 3). Occasionally, a second band of ~65 kDa was also observed, and this probably represents proteolytic products of the Cx–GFP. A similar band was observed when Cx–GFP was expressed in Madin–Darby canine kidney cells (Jordan *et al*., 1999). The wild-type Cx43 (expressed in COS-7 cells) showed a typical pattern of multiple phosphorylation isoforms between ~43 and 50 kDa. Cx32–GFP and Cx26–GFP also expressed proteins of the predicted molecular mass of 59 and 54 kDa in HeLa cells, respectively (our unpublished data).

Because both the numbers and size of the gap junctions vary between cells, the expression of each type of connexin in cultured cells was assessed in terms of percentage area of the cells. The expression of Cx43–GFP ($2.8 \pm 0.2\%$, $n = 15$) was significantly larger than the expression of either Cx32–GFP ($1.2 \pm 0.1\%$, $n = 15$) or Cx26–GFP ($1.0 \pm 0.1\%$, $n = 15$) ($P < 0.0001$ for both), but the expression of Cx26–GFP did not differ significantly from the expression of Cx32–GFP ($P = 0.5$).

The functionality of the gap junctions formed by these chimeric proteins was assayed by their ability to mediate

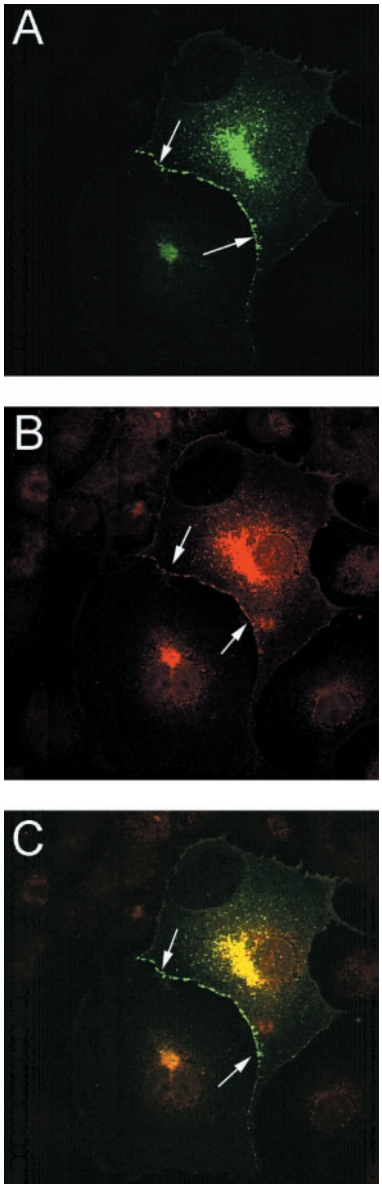

Figure 2. Cellular localization of Cx43–GFP observed by confocal microscopy. (A) A culture of Cx43–GFP-transfected HeLa cells was excited with 450–490 nm light and viewed at 510–520 nm to reveal the location of GFP. Discrete fluorescence plaques, characteristic of gap junctional staining, were observed along the boundary between two cells (arrows). Fluorescence was also detected in the perinuclear region and most likely represents Cx–GFP being processed through the ER. (B) The same area of cells as shown in A stained with Cy3-conjugated antibodies to Cx43 and illuminated at 540–550 nm and viewed at 580–590 nm. A similar staining pattern was observed. (C) The images in A and B were digitally superimposed. The combination of green and red fluorescence results in yellow fluorescence and demonstrates that the membrane plaques and cytoplasmic areas represent sites of colocalization of GFP and Cy3 fluorescence and confirms that GFP fluorescence indicates the location of expressed Cxs. The plaques in C have a green–yellow appearance caused by the larger contribution of green as compared with red. The cells shown were selected for the large number of plaques expressed. For Ca^{2+} experiments, cells with fewer plaques were used. Image width = 60 μm.

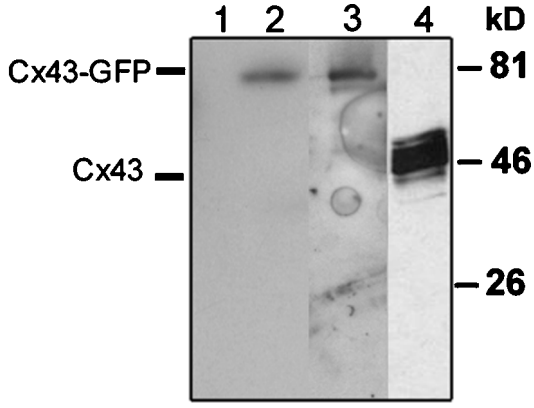

Figure 3. Western blot analysis of Cx43–GFP expressed by mammalian cells. HeLa and COS-7 cells were transiently transfected with 10 μg Cx43–GFP or wild-type Cx43 cDNA, respectively, and were harvested. Cells were dissolved in SDS and analyzed by SDS-PAGE and Western blotting using an antibody to either Cx43 (Gap33) or GFP. Lane 1: control (mock-transfected HeLa cells). Lane 2: HeLa cells expressing Cx43–GFP stained with GFP antibodies. Lane 3: HeLa cells expressing Cx43–GFP stained with Cx43 antibodies. Two major bands are visible. The band at ~71 kDa represents the Cx43–GFP (lanes 2 and 3), whereas the band at ~65 kDa (lane 3) probably represents proteolytic products of Cx43. Lane 4: COS-7 cells expressing wild-type Cx43 stained with Cx43 antibodies. A broad band representing phosphorylated isoforms of Cx43 is evident at ~48–50 kDa. The numbers on the right represent the location and molecular weight (kilodalton) markers.

dye and electrical coupling. Lucifer yellow, microinjected into an individual cell, was subsequently observed in neighboring cells, indicating that all three Cx–GFP chimerae formed dye-permeable gap junction channels (Table 1). Cells expressing Cx43–GFP had generally better dye coupling than the cells expressing Cx32–GFP or Cx26–GFP. Similarly, the injection of 1 nA current into a single cell resulted in synchronous changes in the membrane potential of isolated cell pairs, confirming that the Cx43–GFP cells were electrically coupled (Figure 4). Although multiple GFP-labeled plaques were observed in individual cells, the presence of only one GFP-labeled plaque at the plasma membrane between neighboring cells was sufficient to render the cells

Table 1. Lucifer yellow dye transfer in stable transfected HeLa cells

Cell population	% Cells transferring dye ± SEM (n)
Cx43–GFP	60.25 ± 2.25 (50)
Cx32–GFP	24.6 ± 4.4 (78)
Cx26–GFP	33.2 ± 4 (62)
HeLa control cells	0 (70)

Cells expressing the three Cx–GFP constructs were assessed for their ability to transfer Lucifer yellow. The results are expressed as the percentage of cells transferring dye to five or more cells ± SEM; (n) = total number of cells injected.

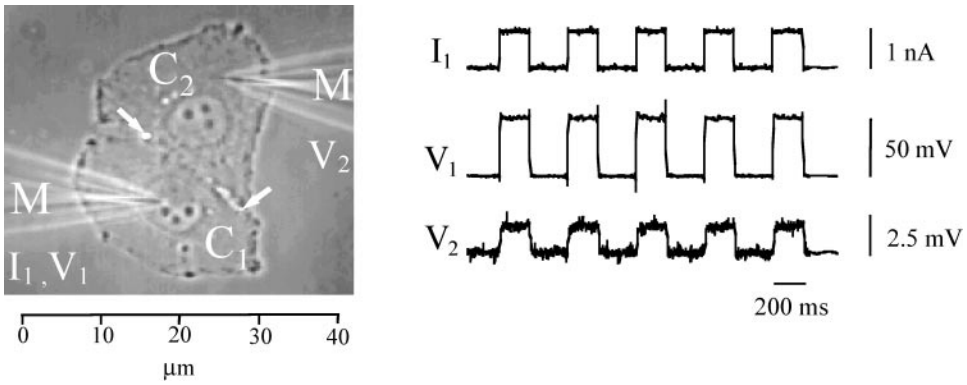

Figure 4. Electrical coupling between isolated pairs of Cx43–GFP-transfected HeLa cells. The left image illustrates a pair of HeLa Cx43–GFP cells impaled with microelectrodes (M) with two gap junctional plaques (white structures or dots) that formed between these cells (white arrows). The image was generated by digitally combining the phase-contrast image of the cells with the fluorescence image of the Cx43–GFP. Cell 1 (C_1) was injected with 1 nA square current pulses of 200 ms duration at a frequency of 2Hz (I_1). The resulting changes in membrane potential in cell 1 (V_1) are synchronous with the changes in membrane potential (V_2) of cell 2 (C_2), indicating electrical coupling between both cells. The coupling ratio (V_2/V_1) is ~5%.

electrically coupled. The coupling ratio of Cx43-transfected cells was ~5%. HeLa control cells were neither electrically nor dye-coupled (Table 1).

The Propagation of Ca^{2+} Waves by ATP

To study Ca^{2+} wave propagation in HeLa cells, cells were loaded with either the fluorescent Ca^{2+}-sensitive indicator fura-2 or fluo-3 and studied by either digital video or high-speed microscopy. Initially Ca^{2+} wave propagation in HeLa control cells was examined. The gentle mechanical stimulation with a glass pipette of a single cell in a confluent layer of cells induced a rise in $[Ca^{2+}]_i$ only in the mechanically stimulated cell (Figure 5A). Increasing the strength or amplitude of the mechanical stimulus induced an increase in $[Ca^{2+}]_i$ in the stimulated cell followed by $[Ca^{2+}]_i$ increases in neighboring cells that propagated in a wave-like manner (Figure 5B). This Ca^{2+} wave propagated at a speed of 10.5 ± 1.1 μm/s and over a distance of >160 μm (n = 5), corresponding to more than six rows of cells.

Because HeLa control cells are not coupled by gap junctions, these experiments suggest that an extracellular factor is involved in Ca^{2+} wave propagation. Other studies have suggested that this factor is ATP (Hassinger *et al.*, 1996; Cotrina *et al.*, 1998; Guthrie *et al.*, 1999). Consequently, the sensitivity of HeLa control cells was tested to a range of ATP concentrations (Figure 6A). HeLa cells were found to have an EC_{50} of 431 nM (95% confidence interval 289–644 nM; R^2 99.7%). An ATP concentration of 10 μM or more increased $[Ca^{2+}]_i$ in all the cells, and this Ca^{2+} response consisted of a rapid increase followed by oscillatory changes of intracellular Ca^{2+} (Figure 7A); however, the presence of the ATP-degrading enzyme apyrase (40 IU/ml) prevented a Ca^{2+} response to 50 μM ATP in 100% of the cells (n = 3) (Figure 7B). By contrast, Ca^{2+} responses to 100 μM histamine were unaffected by extracellular apyrase (n = 3) (Figure 7, C and D). Apyrase was present in the extracellular medium for 30 min before agonist addition but did not cause any Ca^{2+} changes itself (tested up to 1 h).

Because apyrase abolished the effect of ATP on $[Ca^{2+}]_i$, it follows that if Ca^{2+} waves in HeLa control cells are mediated by ATP, apyrase should also abolish or attenuate the Ca^{2+} waves. In the presence of apyrase (40 IU/ml), mechanical stimulation of HeLa control cells induced Ca^{2+} changes that were limited to only the stimulated cell (n = 5) (Figure 5C). Propagated Ca^{2+} changes were observed once, but in this case two neighboring cells showed intracellular Ca^{2+} changes only after a delay of at least 6 s. Normally, Ca^{2+} waves would have propagated >50 μm in this time period.

Analysis with digital high-speed microscopy revealed that, in the absence of apyrase, wave propagation after mechanical stimulation in HeLa control cells initially began with perinuclear Ca^{2+} changes, presumably Ca^{2+} puffs (Thorn *et al.*, 1993; Yao *et al.*, 1995; Bootman and Berridge, 1996), that were followed by a global $[Ca^{2+}]_i$ change, which often appeared as an intracellular Ca^{2+} wave (Figure 8). Although the locations of the perinuclear Ca^{2+} puffs did not correlate with a specific site associated with the nucleus, three-dimensional reconstructions of the ER-Tracker signal showed that ER was invariably present in the perinuclear area (Figure 8). The number of Ca^{2+} puffs preceding global Ca^{2+} changes varied between one and four per experiment (n = 16). The direction of the subsequent intracellular Ca^{2+} wave appeared to be random and not correlated to the interface with the neighboring stimulated cell. A similar high temporal analysis with digital high-speed microscopy of the $[Ca^{2+}]_i$ elevation after exposure to ATP also revealed Ca^{2+} puff-like events preceding a global $[Ca^{2+}]_i$ increase (Figure 6B). These puffs had a $t_{1/2rise}$ of 87.5 ± 21 ms and a $t_{1/2decay}$ of 204 ± 50 ms (n = 6), and their amplitude was ~10% relative change in fluo-3 fluorescence.

Ca^{2+} Waves in Cx–GFP-Transfected Cells

In contrast to the HeLa control cells, mechanical stimulation of a single transfected HeLa cell in a confluent culture in the presence of 40 IU/ml apyrase did evoke propagated Ca^{2+} changes (Figure 9). The numbers of cells participating in

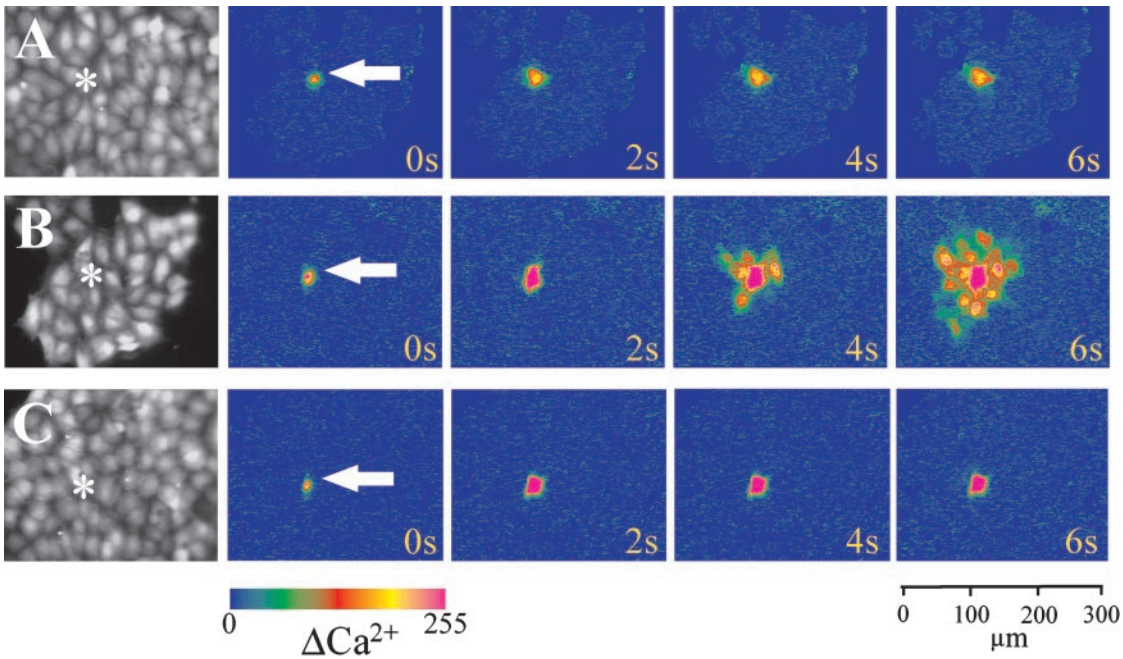

Figure 5. The effects of mechanical stimulation in HeLa control cells using digital video microscopy. The morphology of the cell culture is indicated by the fluorescence of cells loaded with fura-2 (left), and the changes in $[Ca^{2+}]_i$ are indicated by the pseudocolored images (right) (A) A single cell (*, white arrow) was gently stimulated with a glass micropipette. Although this stimulus produced Ca^{2+} changes in the stimulated cell, it did not induce propagated Ca^{2+} changes. (B) Stronger mechanical stimulation of another cell in a different area, induced by distorting the cell to a great extent, initiated propagated Ca^{2+} changes that took the form of a radiating Ca^{2+} wave. (C) The propagating Ca^{2+} changes induced by strong mechanical stimulation were abolished by the presence of 40 IU/ml apyrase in the extracellular solution. The time that each image was recorded after mechanical stimulation is shown in the lower right of each image. Changes of fura-2 fluorescence corresponding to changes in $[Ca^{2+}]_i$ are represented according to a pseudocolor scale bar in arbitrary values.

these waves were significantly smaller than in their counterparts in the absence of apyrase, and propagated Ca^{2+} changes were only observed up to the third row of cells in HeLa Cx43 and up to the second row of cells in HeLa Cx32 and Cx26 ($n = 5$ for each). The average number of cells propagating the Ca^{2+} wave was 4.2 ± 1.0 for HeLa Cx43, 2.4 ± 0.2 for HeLa Cx32, and 2.4 ± 0.4 for HeLa Cx26.

To study the involvement of gap junctions in this type of Ca^{2+} wave propagation in more detail, Ca^{2+} waves induced by mechanical stimulation were examined with digital high-speed microscopy. The localization of the Cx–GFP gap junctions, together with the ER (labeled with ER-Tracker), was three-dimensionally reconstructed from 51 consecutive Z planes that were 0.25-μm apart and encompassed the entire cell thickness (Figure 10). The ER was abundant throughout these cells and invariably present close to the gap junctions (Figure 10). As a control for the ER-Tracker specificity, HeLa cells were loaded with Mito-Tracker. Mitochondria were less abundant in these cells, and their distribution differed significantly. Transfected HeLa cells were mechanically stimulated in the presence of 40 IU/ml apyrase, and the subsequent Ca^{2+} changes were recorded in neighboring cells, at a maximal rate of 100 images per second. Mechanical stimulation induced an intracellular Ca^{2+} wave in the stimulated cell, which spread throughout this cell until it reached the plasma membrane. Subsequent propagation of the Ca^{2+} wave in the neighboring cell was clearly correlated with the location of the Cx–GFP (Figure 10). Delays observed at the site of the gap junction were compared for the three different transfected cell lines and calculated from the difference in time to onset of Ca^{2+} changes in 2.3×2.3 μm analysis points located on either side of the gap junctions (Figure 11). Frequently the delay times could not be measured because they were smaller than the time resolution of 10 ms, and therefore averaging the data was not possible. The range of delays at the site of the gap junction was <10 ms to 90 ms for HeLa Cx26, <10 ms to 156 ms for HeLa Cx32, and <10 ms to 162 ms for HeLa Cx43. The number of gap junctional plaques present at the interface between the two cells was on average 2 ± 0.2 ($n = 22$) for Cx43 plaques, 2 ± 0.2 ($n = 15$) for Cx32 plaques, and 2 ± 0.4 ($n = 10$) for Cx26 plaques.

DISCUSSION

The mechanism underlying the propagation of intercellular Ca^{2+} waves, which occur in various cell types and tissues (Cornell-Bell and Finkbeiner, 1991; Kasai, 1995; Robb-Gaspers and Thomas, 1995; Charles, 1998), has been proposed to occur either by the diffusion of a second messenger (e.g., IP_3) through intercellular gap junctions (Sanderson *et al.*, 1990; Boitano *et al.*, 1992; Hansen *et al.*, 1993; Venance *et al.*, 1997; Leybaert *et al.*, 1998a) or by a factor (e.g., ATP) released into the extracellular space (Hassinger *et al.*, 1996; Cotrina *et al.*, 1998; Guthrie *et al.*, 1999); however, the results of this article demonstrate that in Cx–GFP-transfected HeLa

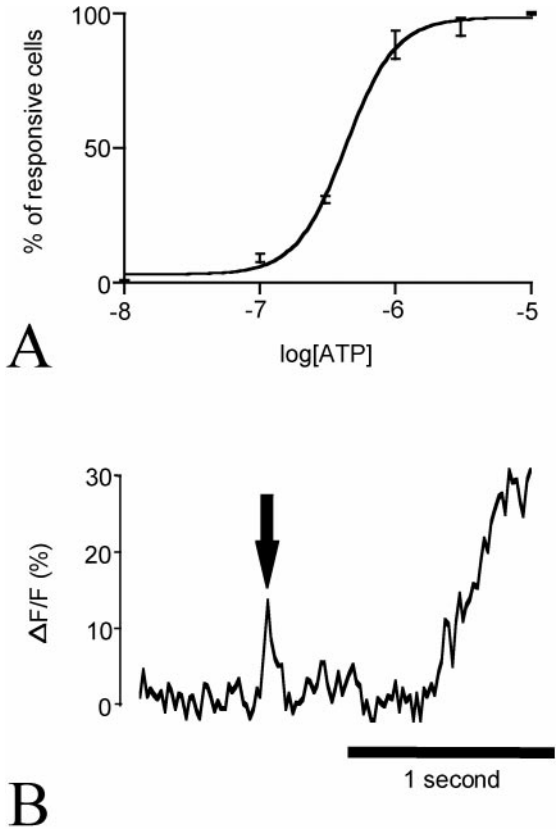

Figure 6. Intracellular Ca^{2+} changes of HeLa control cells in response to ATP. (A) The dose–response curve of the number of HeLa control cells showing an increase in $[Ca^{2+}]_i$ in response to a range of ATP concentrations. Each data point represents the mean (±SE) of three separate experiments and >200 cells. (B) The relative changes in $[Ca^{2+}]_i$ of a HeLa control cell represented by fluo-3 fluorescence in a 2.3 × 2.3 μm (7 × 7 pixels) perinuclear area with respect to time during exposure to 10 μM ATP, which was applied by solution exchange. Before global $[Ca^{2+}]_i$ increases, a much smaller and transient $[Ca^{2+}]_i$ change or Ca^{2+} puff (black arrow) could be observed with digital high-speed microscopy. The Ca^{2+} puff represents a ~10% change in fluo-3 fluorescence.

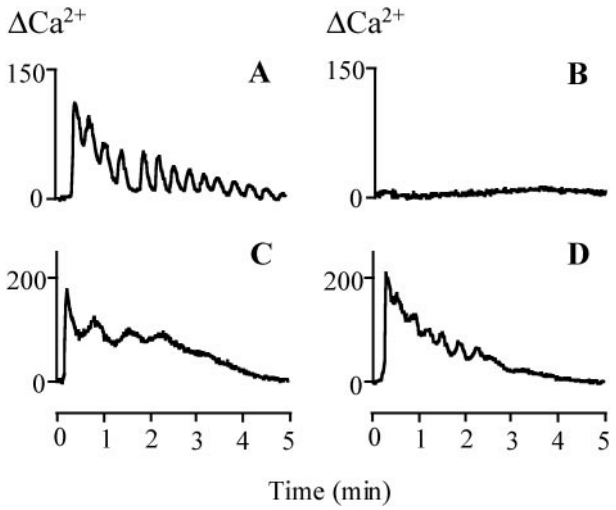

Figure 7. The effect of extracellular apyrase on changes of $[Ca^{2+}]_i$ of HeLa control cells in response to agonists. (A) In the absence of apyrase, fura-2–loaded HeLa control cells respond to 50 μM ATP, added at t = 0 and present throughout the experiment, with an initial Ca^{2+} increase followed by Ca^{2+} oscillations. Time scale bar is indicated at the bottom of the figure. (B) In the presence of 40 IU/ml apyrase, the $[Ca^{2+}]_i$ increase in response to 50 μM ATP is completely abolished. (C) In the absence of apyrase, HeLa control cells also respond to the continuous presence of 100 μM histamine with an initial $[Ca^{2+}]_i$ peak followed by oscillatory changes of $[Ca^{2+}]_i$. (D) In the presence of 40 IU/ml apyrase, the $[Ca^{2+}]_i$ responses to 100 μM histamine are unchanged. The changes in $[Ca^{2+}]_i$ are represented in arbitrary values.

cells, both mechanisms of Ca^{2+} wave propagation, intercellular through gap junctions and extracellular, can coexist.

The use of HeLa cells, an epithelial cell line derived from an epidermoid carcinoma of the cervix, for the study of the relationship between Ca^{2+} signaling and gap junctions has several advantages. HeLa cells have been widely used in the study of Ca^{2+} signaling mechanisms and have been found to possess competent Ca^{2+} signaling machinery (Bootman *et al.*, 1992). HeLa cells have several receptors that are linked to the Ca^{2+} signaling cascade, including the P_2 receptor for phosphorylated nucleotides (e.g., ATP, UTP) and H_2 for histamine (Bootman *et al.*, 1992). The purinoceptor is believed to be P_{2U} on the basis of the nucleotide sensitivity of ATP = UTP > ADP > 2MesATP (Smit *et al.*, 1993). Activation of both P_{2U} and H_2 results in the production of IP_3, which in turn releases Ca^{2+} from intracellular stores formed in the ER (Koch, 1990). The Golgi apparatus and mitochondria also serve as Ca^{2+} stores and contribute to the localization of Ca^{2+} signals in discrete areas of the cytosol (Pinton *et al.*, 1998; Rizzuto *et al.*, 1998). The other advantages of using HeLa cells is that these cells normally express very few, if any, gap junctions and do not display cell coupling (Cao *et al.*, 1998). In addition, this cell line readily tolerates transfection with a wide variety of chimeric proteins (Schroder *et al.*, 1990; Touitou *et al.*, 1990; Graeber and Hulser, 1998). Consequently, these cells were ideal for transfection with plasmids that encode for GFP linked to Cx43, Cx32, or Cx26 so that specific gap junction proteins could be located in living cells and correlated with Ca^{2+} signals.

Mechanical stimulation has been shown to initiate Ca^{2+} waves in a wide variety of cells (Goligorsky, 1988; Sanderson *et al.*, 1990; Frame and de Feijter, 1997; Grandolfo *et al.*, 1998; Himpens *et al.*, 1999). The mechanism propagating these Ca^{2+} waves appears to be the diffusion of IP_3 through gap junctions (Sanderson *et al.*, 1990; Boitano *et al.*, 1992; Hansen *et al.*, 1993; Venance *et al.*, 1997; Leybaert *et al.*, 1998a). The involvement of gap junctions is supported by results showing that C6 glioma cells gained the ability to propagate Ca^{2+} waves after transfection with Cx43 (Charles *et al.*, 1992). In addition, Ca^{2+} wave propagation is not biased by an extracellular fluid flow (Hansen *et al.*, 1993) and can be blocked by gap junction inhibitors in various cells (Enkvist and McCarthy, 1992; Venance *et al.*, 1997); however, in other cell types, mechanical stimulation also appears to initiate the release of ATP from cells, either physiologically or as a result of trauma. The diffusion and perhaps regenerative release of ATP into the extracellular space then leads

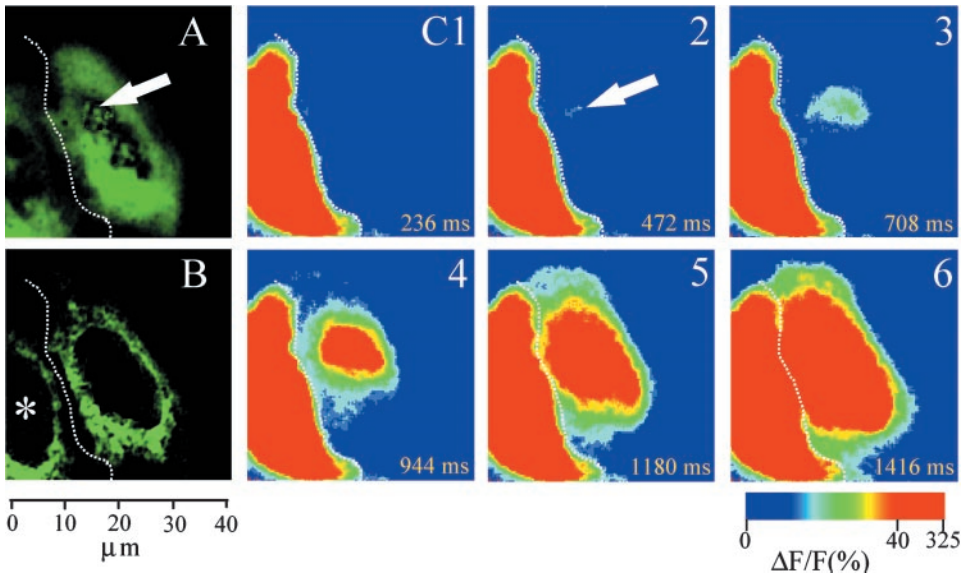

Figure 8. Digital high-speed microscopy of Ca^{2+} waves mediated by an extracellular messenger in HeLa control cells. A and B show the reconstructed ER-Tracker signal (green) in 1-μm-thick slices through the (A) top of the cells and the (B) middle of the cell. The ER surrounds the dark nucleus. No GFP-like fluorescence was detected in these untransfected cells. (C1–C6) A Ca^{2+} wave was evoked, in the absence of apyrase, by mechanically stimulating the cell (*) on the left (B). The propagation of $[Ca^{2+}]_i$ changes in the neighboring cell was initiated by an increase in $[Ca^{2+}]_i$ (white arrow) that was correlated to the supranuclear ER (A, arrow). These initial Ca^{2+} changes were followed by an intracellular Ca^{2+} wave that propagated toward the stimulated cell. Recording times after mechanical stimulation are indicated in the bottom right of each image. The white dotted line represents the cell boundary. Changes of fluo-3 fluorescence at 488 nm excitation, corresponding to changes in $[Ca^{2+}]_i$, are represented in pseudocolor, according to a scale bar. The color scale was chosen to enhance the differentiation of small Ca^{2+} changes. The color scale numbers represent the minimal, saturating, and maximal percentage changes.

to sequential changes in $[Ca^{2+}]_i$ in adjacent cells (Hassinger *et al.*, 1996; Cotrina *et al.*, 1998; Guthrie *et al.*, 1999). Because most mammalian cells express gap junctions and may also release ATP, it has been difficult to determine the predominant mechanism of Ca^{2+} wave propagation.

Because control HeLa cells lack gap junctions, their ability to communicate mechanically stimulated Ca^{2+} waves was more easily assessed. After gentle stimulation, a Ca^{2+} increase occurred only in the stimulated cell; however, heavier stimulation, which was likely to release intracellular ATP, resulted in $[Ca^{2+}]_i$ increases in adjacent cells. High time resolution analysis of these Ca^{2+} waves in HeLa control cells revealed that the changes in $[Ca^{2+}]_i$ frequently were initiated in the form of local Ca^{2+} transients located in a perinuclear position. These Ca^{2+} events are most likely equivalent to Ca^{2+} puffs, as described previously in response to histamine (Bootman and Berridge, 1996), because the stimulating agonist is believed to be IP_3. The Ca^{2+} puffs rapidly grew and coalesced into an intracellular Ca^{2+} wave that spread out toward the cell periphery to bring about a global increase in $[Ca^{2+}]_i$. The direction of travel of the intracellular wave was often back toward the stimulated cell. The idea that the Ca^{2+} waves, resulting from strong stimulation, are mediated by ATP diffusion is also supported by the finding that HeLa control cells displayed Ca^{2+} oscillations in response to ATP. The addition to the medium of apyrase, a mixture of enzymes that degrades ATP to AMP, could abolish both the Ca^{2+} oscillations and the Ca^{2+} wave.

The ability to abolish Ca^{2+} waves in nontransfected cells provided the experimental means to examine the propagation of Ca^{2+} waves via gap junctions in HeLa cells transfected with Cx–GFP. The transfected cells appeared to have functional gap junctions as judged by their ability to demonstrate dye and electrical coupling. Digital high-speed microscopy was used to analyze the three-dimensional distribution of the gap junctions and ER and the propagation of Ca^{2+} changes between cells. High temporal (100 images per second) and spatial resolution (333 × 333 × 250 nm pixel size) reconstructions were obtained by using a short exposure time (possible only with a high-energy laser), a high numerical aperture lens for maximal light collection, a high-speed, low-noise CCD (Rizzuto *et al.*, 1998; Kidd *et al.*, 1999; ZhuGe *et al.*, 1999), and advanced deconvolution software (Carrington *et al.*, 1995).

In the presence of apyrase, mechanically induced Ca^{2+} waves propagated between cells only at points where a Cx–GFP gap junction existed. The route of propagation was often circuitous, as described previously (Sanderson *et al.*, 1990; Charles *et al.*, 1992; Finkbeiner, 1992), and correlated with the presence of gap junctions. Although most cells expressed GFP-labeled gap junctions, cells only participated in a Ca^{2+} wave if the gap junctions faced the adjacent cell showing the Ca^{2+} increase. In the presence of apyrase, Ca^{2+} puffs were not observed, a fact that fits well with the distal location of the perinuclear ER from the gap junction and that an extracellular factor is absent or inactive. The distance of wave propagation in transfected cells also seemed to correlate with the amount of Cx–GFP expression but did not seem to correlate with the type of Cx expressed. This suggests that

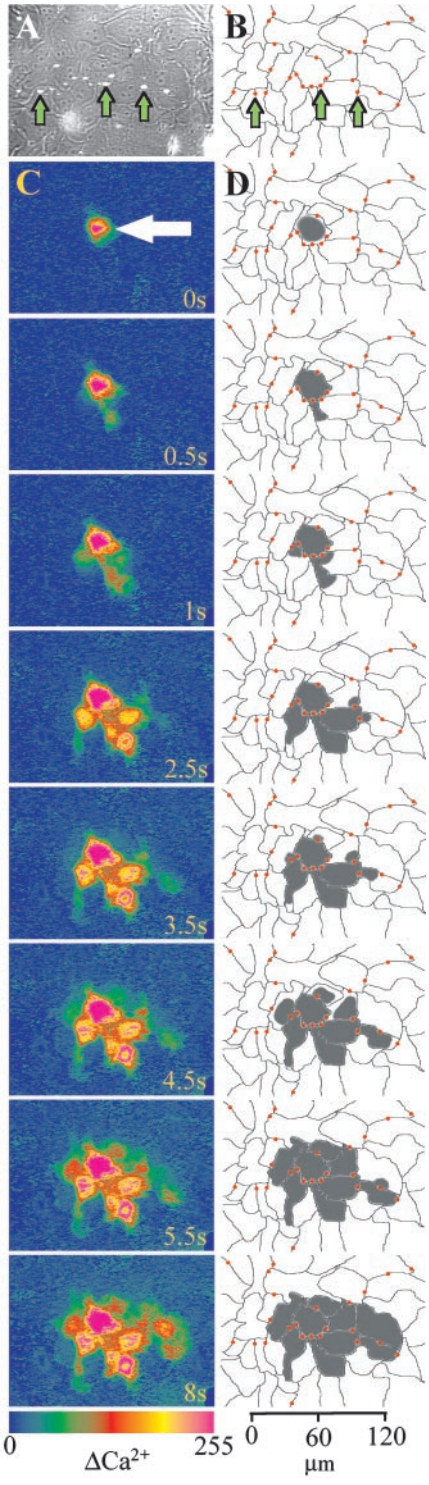

Figure 9. Digital video microscopy of a mechanically induced intercellular Ca^{2+} wave in HeLa cells expressing Cx43–GFP in the presence of 40 IU/ml apyrase. (A) A phase-contrast image of Cx43–GFP HeLa cells superimposed with the corresponding fluorescent image of Cx43–GFP showing plaques of GFP-labeled gap junctions (arrows, white patches) that formed between individual cells. To discard irrelevant background information and before superimposition, the fluorescent GFP image was processed to set the pixel values to black if less than a selected threshold value. (B) An outline of the cell boundaries (gray lines) as well as the positions of the Cx43–GFP plaques (red dots, arrows) were mapped from the phase-contrast and fluorescence images. (C and D) Digital video microscopy of the sequential changes in $[Ca^{2+}]_i$ induced by mechanically stimulating a single Cx43–GFP HeLa cell (white arrow). The time each image was recorded is indicated at the bottom right. The changes in $[Ca^{2+}]_i$ are mapped onto the cell outlines (the expanding gray shaded zone) to correlate the propagation route of the intercellular Ca^{2+} wave with the location of the Cx43–GFP. Close inspection reveals that a Ca^{2+} wave only propagates at sites where two cells are coupled by a gap junction (red dots). Pseudocolor bar represents changes in $[Ca^{2+}]_i$, as measured from the changes in fura-2 fluorescence, in arbitrary values.

Cx43, Cx32, and Cx26 each has similar permeabilities for the diffusing messenger.

These studies in Cx-transfected HeLa cells do not provide additional information on the identity of the internal messenger. Although IP_3 has been shown to be a messenger in previous studies (Sanderson *et al.*, 1990; Leybaert *et al.*, 1998a), the fact that no lag in the propagation of a wave between two cells at the mouth of the gap junction was observed raises the possibility of a rapid local communication by Ca^{2+} itself; however, the gap junctions were always in close proximity to ER, and it is possible that the Ca^{2+} was released from this source through the action of IP_3. It is unclear why substantially longer lag times are observed in other cell types (Sanderson *et al.*, 1990; Robb-Gaspers and Thomas, 1995). One explanation is that the spatial and temporal resolutions, as well as the sensitivity of earlier studies, were insufficient to detect the very early changes at the mouth of the gap junction. An interesting approach for future experiments to determine whether Ca^{2+} itself passes through gap junctions could be to use cells transfected with Cx–aequorin chimeras, which have been shown to report $[Ca^{2+}]_i$ levels at the mouth of the gap junctions (George *et al.*, 1998a).

Other studies investigating Ca^{2+} wave propagation in transfected cells concluded that the forced expression of Cx resulted in the increased ability to release ATP and thereby generate larger Ca^{2+} waves (Cotrina *et al.*, 1998). This hypothesis was based on the ability of cells to release ATP in response to a 30 min stimulation with UTP. How this stimulus correlates to a mechanical stimulus of 150 ms of a single cell is very difficult to interpret. In this study, the presence of extracellular apyrase counters the release of additional ATP by the cells. It is possible that the amount of ATP released would overcome the effects of apyrase; however, the hallmark of ATP-induced waves, i.e., Ca^{2+} puffs and gap junction-independent intercellular Ca^{2+} waves, were not observed. The concentration of apyrase used was able to neutralize the effects of at least 50 μM ATP. Although the concentration of released ATP at the stimulated cell may be high, it would be rapidly diluted by the extracellular space and therefore would be unlikely to stimulate adjacent cells.

In summary, Cx–GFP-transfected HeLa cells have proved to be ideal for the study of the mechanism underlying Ca^{2+} wave propagation. The ability to separate Ca^{2+} changes induced by ATP from Ca^{2+} changes associated with gap junctions leads to

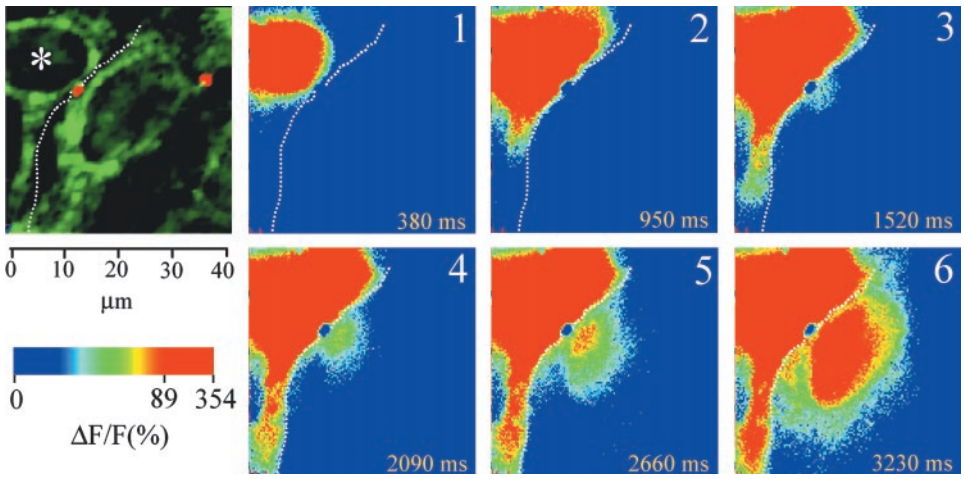

Figure 10. Digital high-speed microscopy of intercellular Ca^{2+} waves in Cx43–GFP HeLa cells. The left top panel shows the distribution of the endoplasmic reticulum and gap junctions reconstructed from ER-Tracker fluorescence (green) and the Cx43–GFP signal (red), respectively, in a 1-μm-thick slice through the cells. A white dotted line represents the cell boundary. The pseudocolored time series of images (right), numbered 1–6, represent the relative changes in fluo-3 fluorescence at the times indicated (bottom right) after mechanical stimulation of a single cell (*) in the presence of extracellular apyrase (40 IU/ml). (1, 2) The Ca^{2+} wave propagates to fill the entire cell in the top left. (3) A small change in $[Ca^{2+}]_i$ is observed in the adjacent cell at the site of the Cx–GFP gap junction. (4–6) The changes in Ca^{2+} continue to spread out from the gap junction. The gap junction remains blue because the GFP fluorescence dominates any Ca^{2+}-based fluorescence changes, and therefore the ratio of $\Delta F/F$ does not change. The color scale was chosen to enhance the visualization of small $[Ca^{2+}]_i$ changes, and numbers represent minimal, saturating, and maximal percentage changes.

the conclusion that mechanically induced Ca^{2+} waves can be propagated simultaneously via an extracellular route or by an intracellular route via gap junctions.

ACKNOWLEDGMENTS

We acknowledge Lawrence Lifshitz (Biomedical Imaging Group, University of Massachusetts Medical School) for assistance in 4D visualization and image analysis using his DAVE software. This work was supported by National Institutes of Health grant HL49288 to M.J.S., a Medical Research Council program grant to W.H.E., and National Science Foundation grants DBI-9724611 and DIR92000027 to R.T., W.C., and K.F. We thank the "De Vooght Foundation" (Belgium) for sponsoring K.P.'s stay at the University of Massachusetts during which this work was completed.

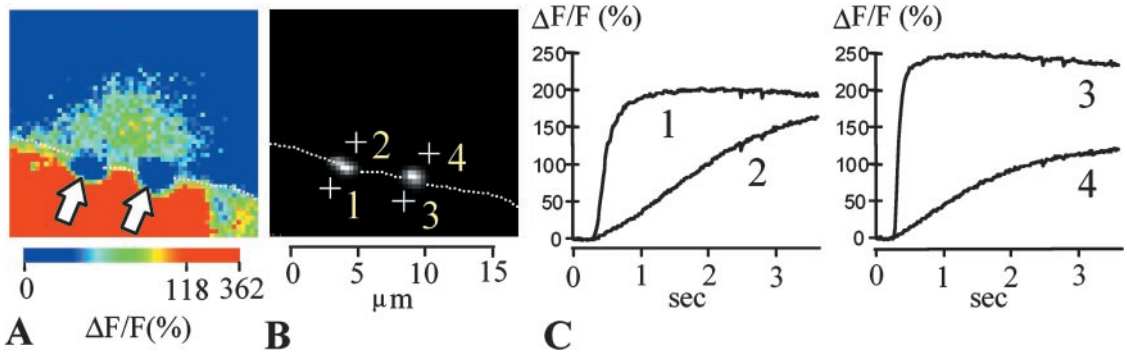

Figure 11. Digital high-speed microscopy of a Ca^{2+} wave induced by mechanical stimulation of a single cell in Cx26–GFP HeLa cells. (A) Ca^{2+} changes in two neighboring cells are analyzed in the vicinity of two gap junctions. The locations of the gap junctions are indicated by the arrows and are derived from B. The color scale was chosen to enhance the visualization of small $[Ca^{2+}]_i$ changes, and the numbers represent minimal, saturating, and maximal percentage changes. (B) The corresponding fluorescent Cx26–GFP image indicates the location of the two gap junctions and the location of the four analysis points (marked with +, area = 2.3 × 2.3 μm) that were used to follow changes in $[Ca^{2+}]_i$ shown in C. The superimposed white line indicates the location of the adjacent plasma membranes. (C) The time course of $[Ca^{2+}]_i$ changes, represented as percentage of relative change of fluo-3 fluorescence, on either side of the two gap junctions at locations 1–4 indicated in B. These traces indicate that the delay times at the site of the gap junctions are very small. The $[Ca^{2+}]_i$ increase on the distal side of the gap junction begins immediately as the $[Ca^{2+}]_i$ is elevated on the near side of the gap junction but takes several seconds to reach a maximal level.

REFERENCES

Boitano, S., Dirksen, E.R., and Evans W.H. (1998). Sequence-specific antibodies to connexins block intercellular calcium signaling through gap junctions. Cell Calcium *23*, 1–9.

Boitano, S., Dirksen, E.R., and Sanderson, M.J. (1992). Intercellular propagation of calcium waves mediated by inositol trisphosphate. Science *258*, 292–295.

Bootman, M.D., and Berridge, M.J. (1996). Subcellular Ca^{2+} signals underlying waves and graded responses in HeLa cells. Curr. Biol. *6*, 855–865.

Bootman, M.D., Berridge, M.J., and Taylor, C.W. (1992). All-or-nothing Ca^{2+} mobilization from the intracellular stores of single histamine-stimulated HeLa cells. J. Physiol. (Lond.) *450*, 163–178.

Cao, F., Eckert, R., Elfgang, C., Nitsche, J.M., Snyder, S.A., H-ulser, D.F., Willecke, K., and Nicholson, B.J. (1998). A quantitative analysis of connexin-specific permeability differences of gap junctions expressed in HeLa transfectants and *Xenopus* oocytes. J. Cell Sci. *111*, 31–43.

Carrington, W.A., Lynch, R.M., Moore, E.D., Isenberg, G., Fogarty, K.E., and Fay, F.S. (1995). Superresolution three-dimensional images of fluorescence in cells with minimal light exposure. Science *268*, 1483–1487.

Charles, A. (1998). Intercellular calcium waves in glia. Glia *24*, 39–49.

Charles, A.C., Merrill, J.E., Dirksen, E.R., and Sanderson, M.J. (1991). Intercellular signaling in glial cells: calcium waves and oscillations in response to mechanical stimulation and glutamate. Neuron *6*, 983–992.

Charles, A.C., Naus, C.C., Zhu, D., Kidder, G.M., Dirksen, E.R., and Sanderson, M.J. (1992). Intercellular calcium signaling via gap junctions in glioma cells. J. Cell Biol. *118*, 195–201.

Churchill, G.C., Atkinson, M.M., and Louis, C.F. (1996). Mechanical stimulation initiates cell-to-cell calcium signaling in ovine lens epithelial cells. J. Cell Sci. *109*, 355–365.

Cornell-Bell, A.H., and Finkbeiner, S.M. (1991). Ca^{2+} waves in astrocytes. Cell Calcium *12*, 185–204.

Cotrina, M.L., Lin, J.H., Alves-Rodrigues, A., Liu, S., Li, J., Azmi-Ghadimi, H., Kang, J., Naus, C.C., and Nedergaard, M. (1998). Connexins regulate calcium signaling by controlling ATP release. Proc. Natl. Acad. Sci. USA *95*, 15735–15740.

Diez, J.A., Ahmad, S., and Evans, W.H. (1999). Assembly of heteromeric connexons in guinea-pig liver en route to the golgi apparatus, plasma membrane and gap junctions. Eur. J. Biochem. *262*, 142–148.

Enkvist, M.O., and McCarthy, K.D. (1992). Activation of protein kinase C blocks astroglial gap junction communication and inhibits the spread of calcium waves. J. Neurochem. *59*, 519–526.

Finkbeiner, S. (1992). Calcium waves in astrocytes: filling in the gaps. Neuron *8*, 1101–1108.

Frame, M.K., and de Feijter, A.W. (1997). Propagation of mechanically induced intercellular calcium waves via gap junctions and ATP receptors in rat liver epithelial cells. Exp. Cell Res. *230*, 197–207.

Furuya, K., Enomoto, K., Maeno, T., and Yamagishi, S. (1993). Mechanically induced calcium signal in mammary epithelial cells. Jpn. J. Physiol. *43*(Suppl 1), S105–108.

George, C.H., Kendall, J.M., Campbell, A.K., and Evans, W.H. (1998a). Connexin-aequorin chimerae report cytoplasmic calcium environments along trafficking pathways leading to gap junction biogenesis in living COS-7 cells. J. Biol. Chem. *273*, 29822–29829.

George, C.H., Martin, P.E., and Evans, W.H. (1998b). Rapid determination of gap junction formation using HeLa cells microinjected with cDNAs encoding wild-type and chimeric connexins. Biochem. Biophys. Res. Commun. *247*, 785–789.

Goligorsky, M.S. (1988). Mechanical stimulation induces $Ca^{2+}{}_i$ transients and membrane depolarization in cultured endothelial cells. Effects on $Ca^{2+}{}_i$ in co-perfused smooth muscle cells. FEBS Lett. *240*, 59–64.

Graeber, S.H., and Hulser, D.F. (1998). Connexin transfection induces invasive properties in HeLa cells. Exp. Cell Res. *243*, 142–149.

Grandolfo, M., Calabrese, A., and D'Andrea, P. (1998). Mechanism of mechanically induced intercellular calcium waves in rabbit articular chondrocytes and in HIG-82 synovial cells. J. Bone Miner. Res. *13*, 443–453.

Grynkiewicz, G., Poenie, M., and Tsien, R.Y. (1985). A new generation of Ca^{2+} indicators with greatly improved fluorescence properties. J. Biol. Chem. *260*, 3440–3450.

Guthrie, P.B., Knappenberger, J., Segal, M., Bennett, M.V.L., Charles, A.C., and Kater, S.B. (1999). ATP released from astrocytes mediates glial calcium waves. J. Neurosci. *19*, 520–528.

Hansen, M., Boitano, S., Dirksen, E.R., and Sanderson, M.J. (1993). Intercellular calcium signaling induced by extracellular adenosine 5′-triphosphate and mechanical stimulation in airway epithelial cells. J. Cell Sci. *106*, 995–1004.

Hassinger, T.D., Guthrie, P.B., Atkinson, P.B., Bennett, M.V., and Kater, S.B. (1996). An extracellular signaling component in propagation of astrocytic calcium waves. Proc. Natl. Acad. Sci. USA *93*, 13268–13273.

Himpens, B., Stalmans, P., Gomez, P., Malfait, M., and Vereecke, J. (1999). Intra- and intercellular Ca^{2+} signaling in retinal pigment epithelial cells during mechanical stimulation. FASEB J. *13*, S63–68.

Jordan, K., Solan, J.L., Dominguez, M., Sia, M., Hand, A., Lampe, P.D., and Laird, D.W. (1999). Trafficking, assembly, and function of a connexin43-green fluorescent protein chimera in live mammalian cells. Mol. Biol. Cell *10*, 2033–2050.

Kasai, H. (1995). Pancreatic calcium waves and secretion. Ciba Found. Symp. *188*, 104–116.

Kidd, J.F., Fogarty, K.E., Tuft, R.A., and Thorn, P. (1999). The role of Ca^{2+} feedback in shaping $InsP_3$-evoked Ca^{2+} signals in mouse pancreatic acinar cells. J. Physiol. (Lond.) *520*, 187–201.

Koch, G.L. (1990). The endoplasmic reticulum and calcium storage. BioEssays *12*, 527–531.

Kumar, N.M., and Gilula, N.B. (1992). Molecular biology and genetics of gap junction channels. Semin. Cell Biol. *3*, 3–16.

Lansley, A.B., and Sanderson, M.J. (1999). Regulation of airway ciliary activity by Ca^{2+}: simultaneous measurement of beat frequency and intracellular Ca^{2+}. Biophys. J. *77*, 629–638.

Leybaert, L., Paemeleire, K., Strahonja, A., and Sanderson, M.J. (1998a). Inositol-trisphosphate-dependent intercellular calcium signaling in and between astrocytes and endothelial cells. Glia *24*, 398–407.

Leybaert, L., Sneyd, J., and Sanderson, M.J. (1998b). A simple method for high temporal resolution calcium imaging with dual excitation dyes. Biophys. J. *75*, 2025–2029.

Martin, P.E., George, C.H., Castro, C., Kendall, J.M., Capel, J., Campbell,, A.K., Revilla, A., Barrio, L.C., and Evans, W.H. (1998). Assembly of chimeric connexin-aequorin proteins into functional gap junction channels. Reporting intracellular and plasma membrane calcium environments. J. Biol. Chem. *273*, 1719–1726.

Osipchuk, Y., and Cahalan, M. (1992). Cell-to-cell spread of calcium signals mediated by ATP receptors in mast cells. Nature *359*, 241–244.

Perez-Terzic, C., Stehno-Bittel, L., and Clapham, D.E. (1997). Nucleoplasmic and cytoplasmic differences in the fluorescence properties of the calcium indicator Fluo-3. Cell Calcium *21*, 275–282.

Pinton, P., Pozzan, T., and Rizzuto, R. (1998). The Golgi apparatus is an inositol 1,4,5-trisphosphate-sensitive Ca^{2+} store, with functional properties distinct from those of the endoplasmic reticulum. EMBO J. *17*, 5298–5308.

Rizzuto, R., Pinton, P., Carrington, W., Fay, F.S., Fogarty, K.E., Lifshitz, L.M., Tuft, R.A., and Pozzan, T. (1998). Close contacts with the endoplasmic reticulum as determinants of mitochondrial Ca^{2+} responses. Science *280*, 1763–1766.

Robb-Gaspers, L.D., and Thomas, A.P. (1995). Coordination of Ca^{2+} signaling by intercellular propagation of Ca^{2+} waves in the intact liver. J. Biol. Chem. *270*, 8102–8107.

Sambrook, J., Fritsch, E.F., and Maniatis, T. (1989). Molecular cloning: a laboratory manual. Cold Spring Harbor, NY: Cold Spring Harbor Laboratory.

Sanderson, M.J. (1995). Intercellular calcium waves mediated by inositol trisphosphate. Ciba Found. Symp. *188*, 175–189.

Sanderson, M.J., Charles, A.C., Boitano, S., and Dirksen, E.R. (1994). Mechanisms and function of intercellular calcium signaling. Mol. Cell. Endocrinol. *98*, 173–187.

Sanderson, M.J., Charles, A.C., and Dirksen, E.R. (1990). Mechanical stimulation and intercellular communication increases intracellular Ca^{2+} in epithelial cells. Cell Regul. *1*, 585–596.

Schroder, H.C., Ugarkovic, D., Merz, H., Kuchino, Y., Okamoto, T., and Muller, W.E. (1990). Protection of HeLa-T4+ cells against human immunodeficiency virus (HIV) infection after stable transfection with HIV LTR-2′,5′-oligoadenylate synthetase hybrid gene. FASEB J. *4*, 3124–3130.

Simon, A.M. (1999). Gap junctions: more roles and new structural data. Trends Cell Biol. *9*, 169–170.

Simon, A.M., and Goodenough, D.A. (1998). Diverse functions of vertebrate gap junctions. Trends Cell Biol. *8*, 477–483.

Smit, M.J., Leurs, R., Bloemers, S.M., Tertoolen, L.G., Bast, A., De Laat, S.W., and Timmerman, H. (1993). Extracellular ATP elevates cytoplasmatic free Ca^{2+} in HeLa cells by the interaction with a 5′-nucleotide receptor. Eur. J. Pharmacol. *247*, 223–226.

Thorn, P., Lawrie, A.M., Smith, P.M., Gallacher, D.V., and Petersen, O.H. (1993). Local and global cytosolic Ca^{2+} oscillations in exocrine cells evoked by agonists and inositol trisphosphate. Cell *74*, 661–668.

Touitou, I., Mathieu, M., and Rochefort, H. (1990). Stable transfection of the estrogen receptor cDNA into HeLa cells induces estrogen responsiveness of endogenous cathepsin D gene but not of cell growth. Biochem. Biophys. Res. Commun. *169*, 109–115.

Toyofuku, T., Yabuki, M., Otsu, K., Kuzuya, T., Hori, M., and Tada, M. (1998). Intercellular calcium signaling via gap junction in connexin-43- transfected cells. J. Biol Chem. *273*, 1519–1528 (erratum *273*, 22856).

Venance, L., Stella, N., Glowinski, J., and Giaume, C. (1997). Mechanism involved in initiation and propagation of receptor-induced intercellular calcium signaling in cultured rat astrocytes. J. Neurosci. *17*, 1981–1992.

Wilkinson, G.W., and Akrigg, A. (1992). Constitutive and enhanced expression from the CMV major IE promoter in a defective adenovirus vector. Nucleic Acids Res. *20*, 2233–2239.

Yao, Y., Choi, J., and Parker, I. (1995). Quantal puffs of intracellular Ca^{2+} evoked by inositol trisphosphate in *Xenopus* oocytes. J. Physiol. (Lond.) *482*:533–553.

Yeager, M., Unger, V.M., and Falk, M.M. (1998). Synthesis, assembly and structure of gap junction intercellular channels. Curr. Opin. Struct. Biol. *8*:517–524.

ZhuGe, R., Tuft, R.A., Fogarty, K.E., Bellve, K., Fay, F.S., and Walsh, J.V., Jr. (1999). The influence of sarcoplasmic reticulum Ca^{2+} concentration on Ca^{2+} sparks and spontaneous transient outward currents in single smooth muscle cells. J. Gen. Physiol. *113*, 215–228.

Zimmermann, B., and Walz, B. (1999). The mechanism mediating regenerative intercellular Ca^{2+} waves in the blowfly salivary gland. EMBO J. *18*, 3222–3231.